Open Access

Non-Invasive Optical Screening of *Streptococcus Pneumonia* Based Inflammatory Changes of the Tympanic Membrane and Mastoid Mucosa in Guinea Pig Otitis Media Using Optical Coherence Tomography

Ruchire Eranga Wijesinghe
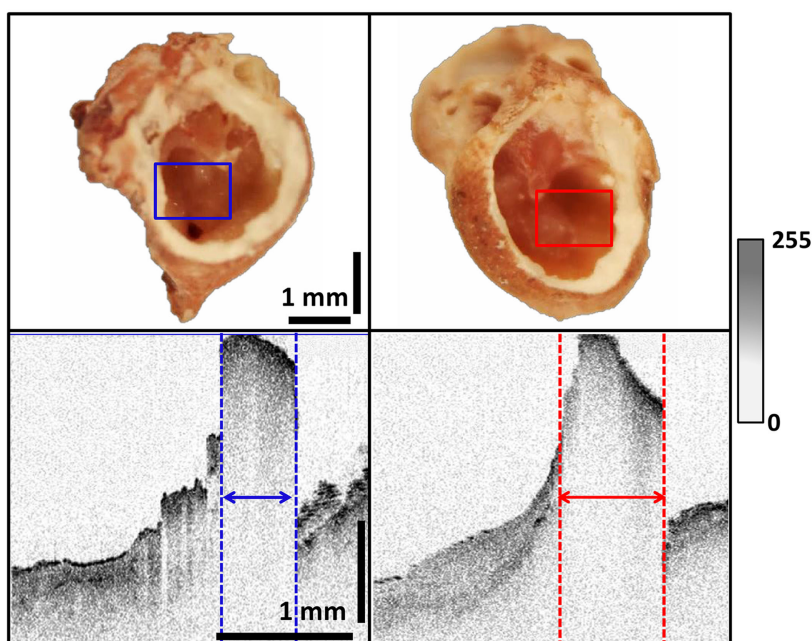Jaeyul Lee
Deokmin Jeon
Pilun Kim
Sangyeob Han
Junsoo Lee
Daewoon Seong
Dong-Eun Lee
Jeong Hun Jang
Mansik Jeon
Jeehyun Kim

Non-Invasive Optical Screening of *Streptococcus Pneumonia* Based Inflammatory Changes of the Tympanic Membrane and Mastoid Mucosa in Guinea Pig Otitis Media Using Optical Coherence Tomography

Ruchire Eranga Wijesinghe,[3,4] **Jaeyul Lee,**[1] **Deokmin Jeon,**[1]
Pilun Kim,[1] **Sangyeob Han,**[1] **Junsoo Lee** ,[1] **Daewoon Seong,**[1]
Dong-Eun Lee ,[5] **Jeong Hun Jang,**[2] **Mansik Jeon** ,[1]
and Jeehyun Kim[1]

[1]School of Electronics Engineering, College of IT Engineering, Kyungpook National University, Daegu 41566, Korea
[2]Department of Otorhinolaryngology-Head and Neck Surgery, School of Medicine, Ajou University, Gyeunggi-do 41944, South Korea
[3]Department of Biomedical Engineering, College of Engineering, Kyungil University, Gyeongsangbuk-do 38428, South Korea
[4]Department of Autonomous Robot Engineering, College of Smart Engineering, Kyungil University, Gyeongsangbuk-do 38428, Korea
[5]School of Architecture and Civil Engineering, Kyungpook National University, Daegu 41566, Korea

Abstract: The accurate screening of otitis media (OM) lies in clarifying the numerous confounding and quantitative factors that are discovered during primary inspections. Increased awareness about bacterial biofilms and inflammation has allowed researchers to develop a better understanding of the bacterial infections that occur in the middle ear. In this study, four live guinea pigs were inoculated with *Streptococcus pneumonia* to induce OM-related inflammatory changes. Since optical techniques have been effectively used for diagnosis in medicine, low-coherence interferometry-based optical coherence tomography (OCT) was employed for depth-resolved high-resolution data screening. Multiple locations of the tympanic membrane (TM), mastoid mucosa, and round window membrane were examined to assess inflammatory changes. We performed qualitative assessments and thickness quantifications and investigated the variations due to adverse inflammatory affects. The findings of the present study provide a better understanding of *S. pneumonia* bacteria caused inflammatory changes in middle ear and it further provides a fundamental platform for future clinical utility.

1. Introduction

Otitis media (OM) of the middle ear is one of the most common diseases observed in otorhinolaryngology [1], [2]. OM can be further classified as chronic OM (COM), OM with effusion (OME), and acute OM (AOM); AOM is an acute infection/inflammation of the middle ear mucosa, which also involves the mastoid hair cells [3]–[6]. Streptococcus pneumoniae (pneumococcus) is the most frequently identified bacterial organism in patients with OM. Moreover, S. pneumoniae is also the main cause for pneumonia and meningitis, especially in children [7], [8].

In otorhinolaryngology clinical conditions are often associated with the development of increased levels of pressure in the middle ear (ME), which may result in the formation of retraction pockets, atelectasis, and cholesteatoma [9], [10]. This can be attributed to impair regulation of ME pressure, which in normal ears, should be maintained close to the ambient or atmospheric pressure. The mastoid cavity has gained more attention as a possible regulatory factor of the overall pressure of ME. The mastoid forms the largest part of the ME, with a distinctly different structure from the tympanum [11]. The mastoid mucosa consists of a thin layer of flat or cuboidal epithelial cells, with loose and highly vascularized subepithelial tissue. These tissue layers are useful for efficient gas exchange. Due to these aspects of anatomy, there is clear and immediate necessity for effective screening of mastoid mucosa and TM with OM inflammatory changes [12].

The otoscope is one instrument that is ubiquitously used in the primary care of OM, which is used to illuminate and magnify surfaces of tissues [13], [14]. Despite the important role of primary care physicians in investigating these tissues, the principal otorhinolaryngological tools have remained largely unchanged for decades. Although the otoscope is used to visualize the surfaces of the oral mucosa, several limitations have been identified in the diagnosis of diseases that occur in sub-surface layers [15]. Alternative techniques, such as acoustic reflectometry [16], tympanometry [17], and Raman imaging [18] have been used to identify inflammatory changes in TM. However, these methods are limited in their visualization of microstructures at a high-resolution and are generally recommended to be used in combination with an otoscope for diagnosis. Since the hallmarks of these diseases are more subtle during the early stages, the existing primary care technologies must be supplemented with non-invasive techniques that are capable of providing more advanced real-time imaging capabilities with high-resolution sub-surface visualization and sufficient quantitative feedback.

OCT is a well-established optical imaging modality based on low-coherence interferometry that is used in biomedical research and in the clinic [19]. OCT enables high-resolution and depth-resolved *in vivo* and *ex vivo* imaging of biological structures through measurement of the echo-time delay, magnitude, and phase of backscattered light. OCT was developed for use in ophthalmology, and has also been extensively used in cardiology, dermatology, gastroenterology, and oncology during the past two decades [20]. Furthermore, OCT has been used to investigate structural and dynamic changes of the ME both *in vivo* and *ex vivo*. The practical use of OCT has been demonstrated in numerous clinical settings showing the potential capability of acquiring quantitative structural information of TM. Several successful middle ear-related OCT studies have been conducted, and have shown the exceptional capabilities of OCT in aiding the identification of sub-surface tissue differentiation and localization of critical structures [21]–[23]. Moreover, the thickness of the TM membrane can be visualized and quantitatively analyzed using OCT to delineate the relevant morphological structures [24]–[26]. Pre-identification of these morphological changes *in vivo* at an early stage not only offers a value from a research point of view, but may also be beneficial to understanding the changes that occur during the process of infection. This information is essential to halting the development of a bacterial biofilm in the ME.

In this study, we present an OCT-based morphological and quantitative approach to obtain thickness measurements as a method of assessing inflammatory changes that occur early in mastoid mucosa and TM with OM after the inoculation of *S. pneumonia*. Our results demonstrate
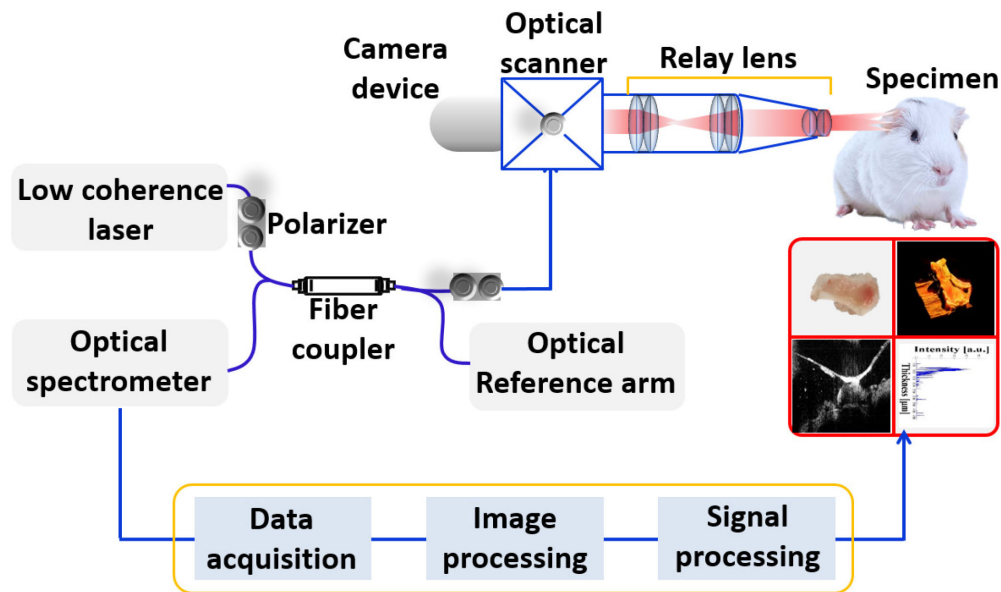
Fig. 1. System configuration of the OCT-based inspection modality.

that the use of OCT allows for immediate visualization of the ME, providing a precise qualitative comparison between control and abnormal infected mastoid mucosa and TM regions after the inoculation of *S. pneumonia*, which is yet to be reported in OCT literature. A pixel intensity-based thickness tracking algorithm was employed to gain a better understanding of TM and mastoid mucosa thickness variations, providing a quantitative method to screen the OM non-invasively. Therefore, this study provides novel insight into the morphological changes that occur due to *S. pneumonia*-associated inflammation in the mastoid mucosa and TM. Future clinical studies can use this methodology to assess these changes in patients in the clinic.

2. Experimental Materials

2.1 Optical Inspection System Configuration

Schematic of the OCT system configuration is shown in Fig. 1. The system was operated using a broadband light source (BroadLighters T-860-HP, Superlum) with a center wavelength of 860 nm and a full width at half maximum of 165 nm. A 50:50 optical fiber coupler split the laser beam into sample and reference arms. The interference fringes of the backscattered beam from the sample and reference arms were recorded using a compact spectrometer. A pair of prisms was connected in the reference path to compensate for the dispersion within the optics of the sample path. The inspection sample arm consisted of a collimator, galvanometer scanner, objective lens, and relay lenses to obtain cross-sectional images. The axial resolution and the signal-to-noise ratio were improved by calibrating the optical spectrum, as described previously [27]. The axial and lateral resolutions measured (in air) of the system were 5 μm and 16 μm, respectively. High-resolution video and color images of the examined mastoid mucosa and TM regions were acquired using a miniaturized commercially available high-resolution optical microscope integrated charge-coupled device video camera with 1.3 megapixels. The system processing methods and the detailed configurations of the OCT instrumentation used were described previously [28], [29].
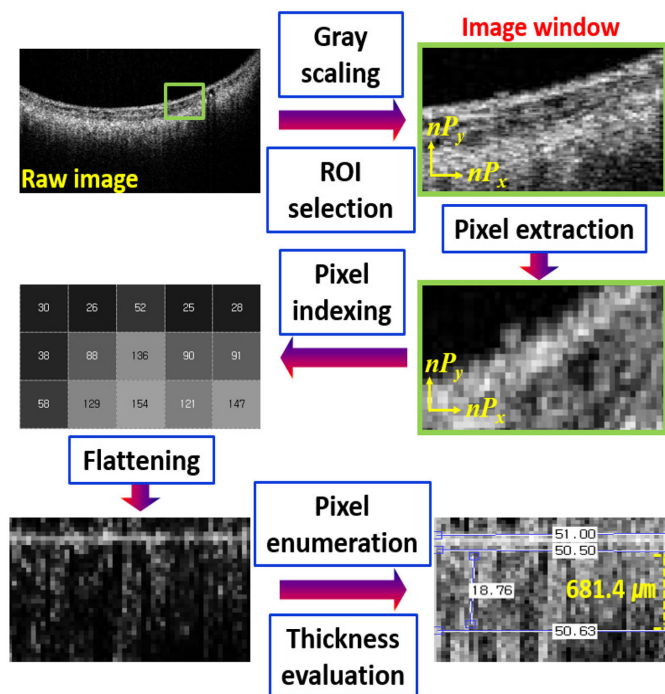
Fig. 2. Graphical representation of OCT pixel enumeration-based thickness measurement procedure.

2.2 Preparation of the Animal Model of OM

All animals were managed in compliance with the Guidelines for the Care and Use of Laboratory Animals of the National Institutes of Health, and all experiments were performed according to the Guidelines of the Internal Animal Care and Use Committee of Ajou University Hospital Biomedical Research Institute (approval no. 2016–0027). Five Harley Albino guinea pigs (255–455 g) aged 7–9 weeks were used. During the experiment, four animals were inoculated, and the remaining animal served as a control. After delivery of general anesthesia, ketamine (90 mg/kg) and xylazine (10 mg/kg), an incision about 1.5 cm in length was made in the retroauricular area of left ear. The location of the bulla was confirmed via palpation of bony protrusions in the posterior inferior part of the skull. The muscle fascia and the periosteum were removed with scissors and forceps. After confirming the triangular shape of the external surface of the bulla, a pinhole sized bullotomy was performed using a Rosen pick. *Streptococcus pneumoniae* was inoculated into the ME using a bulla pinhole and a 24-gauge needle connected to a 1 cc syringe. After injection, the bullotomy site was covered with gelfoam, and muscle closure was performed. To minimize mortality and morbidity, all animals were kept on warm platforms. The animals were examined 7 days after the inoculation. Transcardiac perfusion with phosphate-buffered saline was performed prior to the dissection. The bulla was isolated from the skulls and was divided into the large pieces using a drill with a 1 mm-diamond burr. The images of the ME mucosa inside the bulla were obtained using the OCT system.

2.3 Pixel Enumeration-Based Thickness Measurement Procedure

Fig. 2 describes the laboratory customized OCT pixel enumeration-based thickness measurement procedure for the inflammatory changes that occurred in multiple locations of the TM and mastoid mucosa. To evaluate total pixel intensity-based depth dependent intensity fluctuation, a concise program was coded using MATLAB (Mathworks, USA). First, raw images (two dimensional (2D)-OCT images) were loaded into the program and a median filter was applied to compensate the speckle noise of cross-sections. As the secondary step, this post-processing method consists of an image

window with adjustable dimensions to evaluate thickness information by selecting the infected or abnormal region of interest (ROI), where the remaining regions, which do not represent inflammatory changes can be discarded according to the surgeon's point-of-view. Although this manually functioned image window selection is an arbitrary process, the dimensions of this software-based imaged window size is adjustable accordingly without any shortage of missing infected or apparently abnormal morphological structures including non-flattened or curved structures owing to the physiological nature of the TM as emphasized in Fig. 2. The relative dimensions are described as nP_x (X-direction) and nP_y (Y-direction).Thus, the challenge of measuring approximate layer thickness considering the variability of depth signals was able to be rectified. Though each component of a tissue has a unique refractive index, herein, a refractive index of 1.32 (fundamental average refractive index of TM and surrounding structures) was applied to the entire image window. Since 2D-OCT images are composed with axial direction depth profiles (depth A-scans), each A-scan of 2D-OCT image corresponds to a vertical direction pixel array. Hence, the number of vertical pixel arrays of manually functioning arbitrarily selected image window is different at each attempt. Next, the number of pixels and pixel-intensity values of the image window were extracted and arranged in a sequential manner. To detect the peak pixel intensity (gray scale intensity of OCT images) in each pixel array, a peak pixel intensity search function was simultaneously simulated. The peak pixel intensity search function detects the maximum pixel intensity in each individual pixel array sequentially. Then all the peak pixel intensity value positions in each vertical pixel array of the entire selected image window were rearranged. Although in OCT, it will be the intensity with largest gradient, rather than maximum intensity value that correspond to the topmost layer, the physical nature of TM, mastoid mucosa, and round window membrane illustrate non-flattened 2D OCT cross-sectional images containing maximum pixel intensity index positions at different positions located in vertical pixel arrays. Therefore, the index positions with the maximum pixel intensity should be rearranged and matched linearly to obtain a flattened image. Once curved structures are successfully flattened, the number of pixels, which are included in the image window emphasizing the ROI were enumerated and fully considered for the thickness evaluation.

3. Results

3.1 Preparation of the Animal Model of OM

Fig. 3(a)–(d) shows representative 2D-OCT images of *ex vivo* TM acquired from four *S. pneumonia*-inoculated guinea pig models of disease. Prior to perform OCT imaging, the specimens were initially examined 7 days after the disease inoculation by an expert Otorhinolaryngology surgeon. The disease progression as well as the structural changes of normal ME tissues were confirmed through high-resolution optical microscope integrated camera visualizations and previous OCT assessments [30], [31]. The acquired 2D-OCT visualizations clearly emphasized the biofilm growth due to disease progression with a structural comparison between healthy homogenous structures (indicated with yellow color vertical dashed lines) and infected heterogeneous structures (indicated with white color vertical dashed lines) through structural abnormalities with a biofilm growth. Therefore, white dotted squares on the 2D-OCT images correspond to the formation of abnormalities, while the yellow color vertical lines indicate regions without any thickness discrepancies prior to the spread of infection, which are apparent non-infected regions. The thickness measurements were obtained from all locations, which are graphically illustrated in Fig. 3(e)–(h). Noticeable differences were observed in the TM after the inoculation, which were precisely visualized through 2D-OCT images that were captured. Interestingly, there were clearly identifiable areas with initial formation of a biofilm in regions of the TM. These areas had higher scattering intensity than the non-infected regions, which were mapped at intensity between 0 and 255. The 2D-OCT data acquired from TM regions was subsequently used to determine the thicknesses of the abnormal regions. The average thickness values were calculated using an image window with 50 intensity lines (shown in the dotted square region) for both non-infected and infected regions. As described in the measurement procedures, the angled TM geometry was mathematically indexed and flattened to
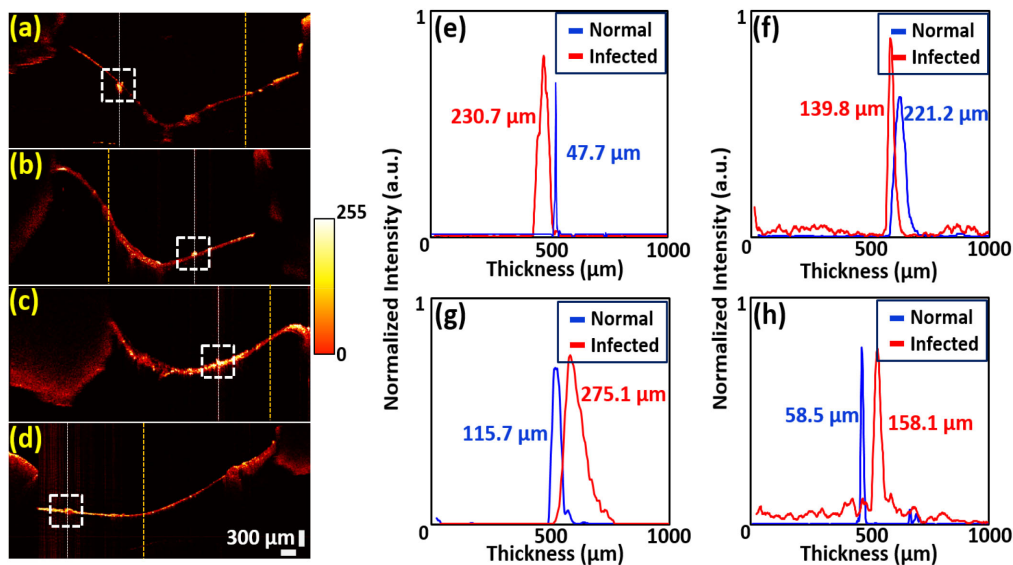
Fig. 3. (a)–(d): Representative depth-resolved 2D-OCT images of multiple TM regions. (e)–(h): Quantitative thickness comparisons between normal and infected regions.

obtain accurate thickness readings. The depth profiles shown in Fig. 3(e)–(h) quantify the thickness differences between the uninfected and abnormal locations, as indicated on the cross-sections. When the depth profiles are displayed on the same intensity and depth scales, the abnormal regions typically exhibit a higher thickness and normalized intensity in comparison with non-infected regions. Although qualitative appearance-based diagnosis based on physical appearance has been the conventional diagnostic parameter, the quantifications that we have developed significantly enhance diagnosis accuracy.

3.2 Non-Invasive Classification of the Mastoid Bone

The OM and COM are the stages of ear disease in which there are inflammatory changes of the TM and mastoid bone in the ME. Therefore, as a secondary inspection approach, the mastoid mucosa region was examined in all four *S. pneumonia*-inoculated guinea pigs. Fig. 4(a) and 4(b) illustrate the gray-scaled and color-scaled intensity representations of the mastoid mucosa, which were visualized using a high-resolution optical microscope integrated camera. Particular regions with OM, infected regions, and apparently normal regions are indicated with red, yellow, and magenta colored arrows, respectively. Fig. 4(c) shows the 2D-OCT representation acquired from an apparently normal structural region of black dashed circular region of Fig. 4(b), which consists of abnormal and apparently normal regions. The blue color horizontal dashed line indicates the exact scanned location. On the right side, median thickness values are indicated on the 2D-OCT images (Fig. 4(h)–(k)) corresponding to the regions of interest indicated on the optical microscope integrated camera images (Fig. 4(d)–(g)). The numerical results show that all of the mastoid bones have an equal variance with an increased thickness coefficient. In contrast, optical microscope integrated camera images provide a cloudy dark red appearance due to inflammation. The acquired qualitative and quantitative assessments reveal that the thickness of the infected regions is 1.5 times greater than that of the normal regions, which confirms the natural progression of inflammation. Since the guinea pig bulla specimens were surgically extracted and were examined in *ex vivo* state, the thickness expansion of mastoid bony regions and surroundings were satisfactorily visualized qualitatively and quantitatively owing adequate penetration of OCT beam towards the mastoid bony regions.
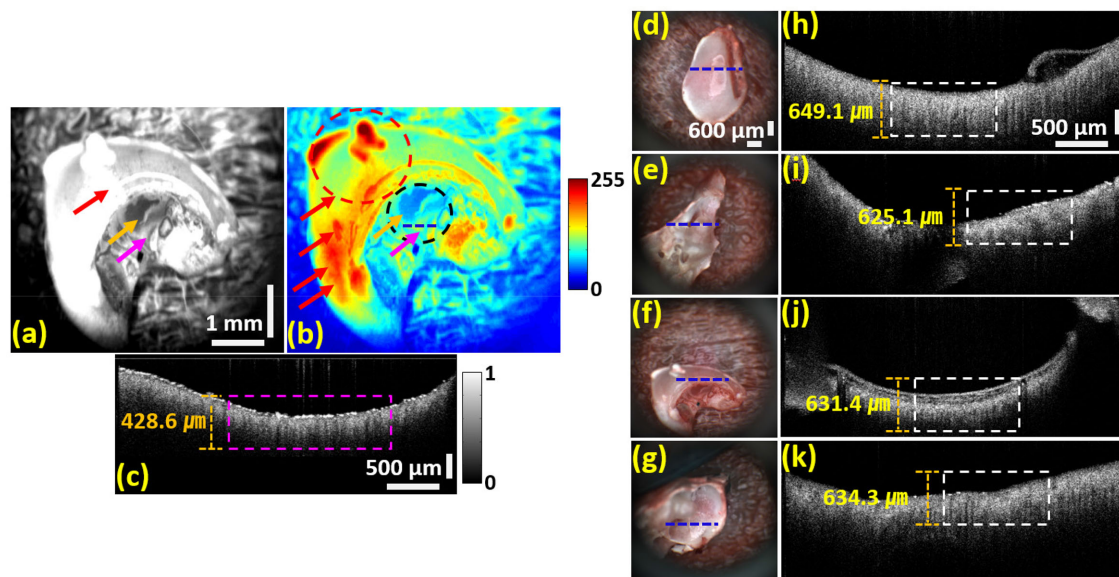
Fig. 4. (a)–(d) (a, b): Gray-scaled and color-scaled intensity representations of the mastoid mucosa. (c): 2D-OCT representation acquired from the apparently normal region (indicated with blue color horizontal dashed line) of black dashed circular region of Fig. 4(b), (d)–(g): Microscopic visualization of the infected mastoid mucosa regions. (h)–(k): Corresponding OCT cross-sections acquired from blue colored dashed line region indicated on the optical microscope integrated camera images.

3.3 Cross-Sectional Assessment of Round Window Membrane

Inflammatory changes can occur in the round window membrane as result of OM. Since the oval window and round window membrane are connected to the cochlea, these structural transformations must be classified. Thus, diagnosis of the round window membrane was performed using the four inoculated guinea pigs. The main difficulty of inspecting the round window membrane is the destruction of the inner ear, as membrane removal leads to destruction of the cochlea. Therefore, intraoperative isolation of the round window membrane was performed. Fig. 5(a)–(d) depicts the cross-sectional representation of the four round window membranes that were examined, where the white colored dashed boxes emphasize the regions of interest in each cross-section. Fig. 5(e)–(h) shows the zoomed visualizations of the regions of interest. The angled slices of the round window membranes were selected for thickness determination in the illuminated regions of interest. Software-based boundary detection was performed assess the exact morphological boundary region, indicated by the red colored solid line for each round window membrane. The green and red colored dashed lines illustrate a comparison of thicknesses between normal regions and infected regions, respectively. Five locations from both the green and red dashed regions were acquired and averaged to obtain corresponding thickness values for both the normal and infected regions. The measured mean thickness range of normal regions was 10–30 μm and infected regions were 80–200 μm. The axially confined thickness distribution identified through OCT visualization confirmed the diagnostic capability of OCT.

Table 1 illustrates the averaged thicknesses of the TM, mastoid mucosa, and round window membrane in non-infected and infected regions. There were reductions in thickness of microstructures due to disease progression.

4. Discussion

Pre-diagnosis of OM is challenging due to the difficulties in acquiring morphological information [32]. Therefore, many studies have utilized a combination of microscopy and optical coherence
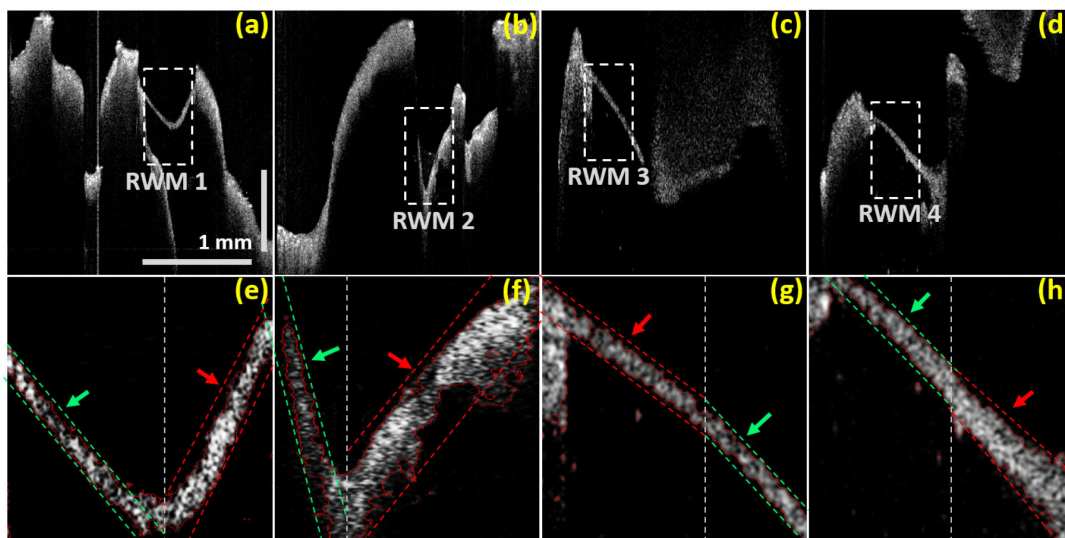
Fig. 5. Cross-sectional analysis and structural classification of normal and infected regions after the inoculation of *Streptococcus pneumonia*. The green dashed lines and green arrows illustrate normal regions and red dashed lines and red arrows illustrate infected regions. RWM: round window membrane.

TABLE 1

Summary of Averaged Non-Infected and Infected Thicknesses for TM, Mastoid Mucosa, and Round Window Membrane

Sample status	Tympanic membrane	Mastoid mucosa	Round window membrane
Non-infected regions	82 μm (n = 1)	544.5 μm (n = 1)	24.8 μm (n = 1)
Infected	176.3 μm (n = 4)	634.9 μm (n = 4)	157.5 μm (n = 4)

tomography imaging to gain a higher depth-resolved sensitivity [30], [33], [34]. In the current study, technological integration-based qualitative and quantitative measurements of *S. pneumonia*-inoculated guinea pig ME specimens were acquired to examine inflammatory changes that occur in the TM and mastoid bone after the inoculation of disease. Collectively, qualitative 2D-OCT assessments and pixel-intensity based thickness evaluations provided compelling evidence for the presence of structures with biofilm growth and disease progression-based thickness increase of the examined regions. To obtain further confirmation and morphological classification, non-infected and infected mastoid bone regions were examined through the acquired cross-sections. In fact, the primary goal of the demonstration was to confirm the structural abnormalities of TM, mastoid mucosa, and round window membrane due to disease progression after the inoculation using OCT. However, the acquisition of OCT visualizations of *in vivo* normal regions was a challenging task using the employed OCT system configuration. Since the OCT assessments of the current study clearly revealed the biofilm growth due to disease with a structural comparison between healthy homogenous structure and infected heterogeneous structure through structural abnormalities (with a biofilm growth), the comparison between healthy and infected were conducted using the obtained raw *ex vivo* OCT visualizations, while supportive literature reports emphasizing healthy *in vivo* structures of the examined regions, which were acquired using handheld-OCT and surgical-OCT maneuvers can be referred elsewhere [26], [29], [35]–[38]. Fig. 6(a) shows the mastoid bony regions extracted from the control guinea pig along with a representative cross-sectional visualization (Fig. 6(b)–(d)). The horizontal dotted lines of Fig. 6(a) and 6(b) represent the regions of interest.
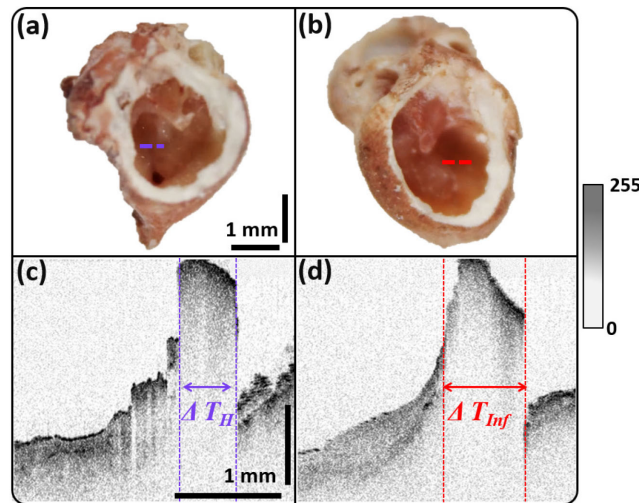
Fig. 6. Morphological comparison between surgically extracted non-infected and infected mastoid mucosa bony regions. (a and b): Top view of the non-infected and infected mastoid mucosa bony regions. (c and d): Corresponding cross-sectional images acquired from the dotted lines indicated on (a) and (b). The dimensions of the lateral purple and red arrow signs indicated on (c) and (d) images reveal the thickness differences between non-infected regions and abnormal bony structures.
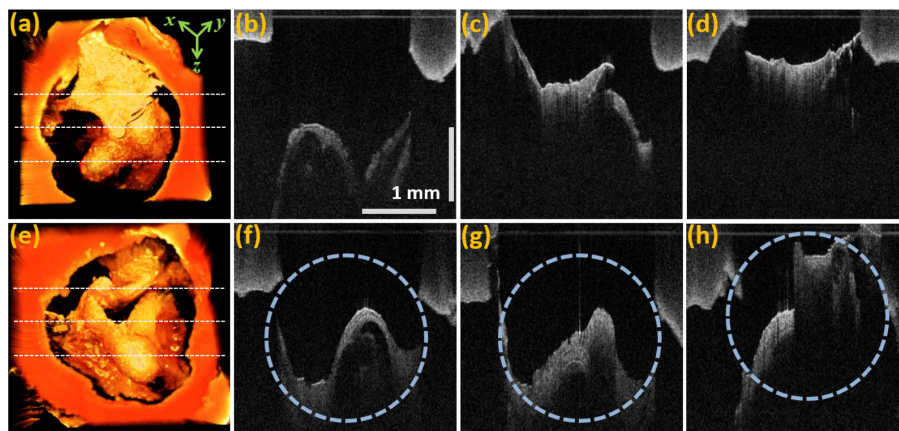

Fig. 7. (a and b): volumetric assessments acquired from the surgically extracted non-infected and infected mastoid mucosa bony regions. The corresponding multiple cross-sectional images acquired from the dotted regions were used to confirm the cross-sectional difference between non-infected and infected regions.

Clearly identifiable thickness comparison can be observed between two specimens (indicated with purple and red color bi-directional arrows), and the thickened bony structure of the infected mastoid bone (indicated with solid bi-directional red color arrow) reveals the progression of infection in the diseased animal model.

Moreover, 3D-OCT images were constructed to obtain volumetric assessments, as shown in Fig. 7. The representative volume renders of the mastoid bony region of the diseased animal model (Fig. 7(e)–(h) confirm the growth of biofilm regions, which are indicated with the blue colored dashed circles, as compared to the control mastoid bony region (Fig. 7(a)–(d). Since guinea pig TM and ME structures are similar to those of human ears, the acquired 2D and 3D-OCT visualizations provide a convincing platform to confirm the potential merits of this method. Therefore, the results of this pre-clinical animal study demonstrate the potential use and provide a new insight for research and clinical use for diagnosis of *S. pneumonia* bacteria-infected OM.

The *ex vivo* specimens of the study were examined 7 days after the disease inoculation by an expert Otorhinolaryngology surgeon, while the formation of abnormalities were visually examined and confirmed through a conventional high-resolution optical microscope integrated camera based imaging technique, and simultaneously verified through the histological representations along with quantitative assessments of previous literature reports [18], [39], [40]. The obtained 2D-OCT images based numerical assessments shown in Table 1 revealed a significant increase in infected structural thickness of round window membrane (approximately 6 times greater than normal region) and TM (approximately 2 times greater than normal region) in comparison with mastoid mucosa. The fundamental scope of this study was to investigate how feasible and beneficial is OCT to diagnose inflammatory changes that occur early in mastoid mucosa, TM, and round window membrane with OM after the inoculation of *S. pneumonia*. Therefore, a less number of *ex vivo* specimens were involved in this study preliminarily. Although the number of specimens is less, the feasibility was sufficiently confirmed through the obtained quantitative and qualitative results and precisely verified with previously reported histological and quantitative assessments [18], [30], [31], [40]–[42]. Nevertheless, using the current results to determine a threshold parameter confirmed through a *P value* analysis is challenging due to the lack of *in vivo* assessments. Therefore as the base demonstration to assess clinical applicability, it is worthy to note that successive *in vivo* clinical trials with extensive quantifications will be extraordinarily beneficial to obtain highly accurate threshold parameters to diagnose inflammatory changes occur in middle ear.

5. Conclusion

This study demonstrates a non-invasive quantitative method to identify fundamental morphological changes of the TM, mastoid mucosa, and round window membrane in response to *S. pneumonia* bacterial infection *ex vivo*. Cross-sectional images were acquired from multiple locations of these structures to observe structural changes. The customized pixel intensity-based thickness tracking algorithm was utilized to confirm structural changes. To further confirm these findings, surgically extracted non-infected and infected mastoid mucosa specimens were examined under *ex vivo* conditions to further confirm biofilm growth after inoculation. The qualitative 2D and 3D image-based findings successfully confirmed the disease growth in middle ear structures; therefore, OCT provides a means to rapidly and non-destructively assess abnormalities in the TM and mastoid mucosa. These findings suggest the usefulness of using both high-resolution OCT and endoscopy, rather than invasive sampling, to perform a multi-dimensional inspection of ME diseases at an early stage.

References

[1] M. M. Rovers, A. G. Schilder, G. A. Zielhuis, and R. M. Rosenfeld, "Otitis media," *Lancet*, vol. 363, pp. 465–473, 2004.

[2] A. G. Schilder *et al.*, "Otitis media," *Nature Rev. Disease Primers*, vol. 2, 2016, Art. no. 16063.

[3] H. Atkinson, S. Wallis, and A. P. Coatesworth, "Otitis media with effusion," *Postgraduate Medicine*, vol. 127, pp. 381–385, 2015.

[4] A. Górecka-Tuteja, I. Jastrzębska, J. Składzień, and K. Fyderek, "Laryngopharyngeal reflux in children with chronic otitis media with effusion," *J. Neurogastroenterology Motility*, vol. 22, 2016, Art. no. 452.

[5] J. Nokso-Koivisto, T. Marom, and T. Chonmaitree, "Importance of viruses in acute otitis media," *Current Opinion Pediatrics*, vol. 27, 2015, Art. no. 110.

[6] S. Val, "Basic science concepts in otitis media pathophysiology and immunity: Role of mucins and inflammation," in *Otitis Media: State of the Art Concepts and Treatment*. Berlin, Germany: Springer, 2015, pp. 53–77.

[7] D. Bogaert, R. de Groot, and P. Hermans, "Streptococcus pneumoniae colonisation: The key to pneumococcal disease," *Lancet Infectious Diseases*, vol. 4, pp. 144–154, 2004.

[8] P. C. Appelbaum, "Antimicrobial resistance in Streptococcus pneumoniae: An overview," *Clin. Infectious Diseases*, vol. 15, pp. 77–83, 1992.

[9] P. V. F. Jensen and M. Gaihede, "Congestion of mastoid mucosa and influence on middle ear pressure–Effect of retroauricular injection of adrenaline," *Hearing Res.*, vol. 340, pp. 121–126, 2016.

[10] F.-M. Gu and F.-L. Chi, "Titanium ossicular chain reconstruction in single stage canal wall down tympanoplasty for chronic otitis media with mucosa defect," *Amer. J. Otolaryngology*, vol. 40, pp. 205–208, 2019.

[11] C.-Y. Kuo *et al.*, "Surgical results of retrograde mastoidectomy with primary reconstruction of the ear canal and mastoid cavity," *BioMed. Res. Int.*, vol. 2015, pp. 1–12, 2015.

[12] P. Marchisio *et al.*, "Prospective evaluation of the aetiology of acute otitis media with spontaneous tympanic membrane perforation," *Clin. Microbiol. Infection*, vol. 23, pp. 486.e1–486.e6, 2017.

[13] J. Classen, A. Bruehschwein, A. Meyer-Lindenberg, and R. Mueller, "Comparison of ultrasound imaging and video otoscopy with cross-sectional imaging for the diagnosis of canine otitis media," *Veterinary J.*, vol. 217, pp. 68–71, 2016.

[14] N. Bedard *et al.*, "Light field otoscope design for 3D in vivo imaging of the middle ear," *Biomed. Opt. Express*, vol. 8, pp. 260–272, 2017.

[15] B. Yazici, H. Sabur, and N. Orucov, "Use of direct otoscope for intranasal examination after dacryocystorhinostomy," *Ophthalmic Plastic Reconstructive Surgery*, vol. 32, pp. 116–117, 2016.

[16] N. Erkkola-Anttinen, M. K. Laine, P. A. Tähtinen, and A. Ruohola, "Can changes in parentally measured acoustic reflectometry levels predict the middle ear status?" *Int. J. Pediatric Otorhinolaryngology*, vol. 95, pp. 72–74, 2017.

[17] B. Sackmann, E. Dalhoff, and M. Lauxmann, "Model-based hearing diagnostics based on wideband tympanometry measurements utilizing fuzzy arithmetic," *Hearing Res.*, vol. 378, pp. 126–138, Feb. 28, 2019.

[18] S. Singh *et al.*, "Identification of early inflammatory changes in the tympanic membrane with Raman spectroscopy," *Analyst*, vol. 144, pp. 6721–6728, 2019.

[19] D. Huang *et al.*, "Optical coherence tomography," *Science*, vol. 254, pp. 1178–1181, 1991.

[20] A. C. Tan *et al.*, "An overview of the clinical applications of optical coherence tomography angiography," *Eye*, vol. 32, 2018, Art. no. 262.

[21] G. L. Monroy *et al.*, "Noninvasive depth-resolved optical measurements of the tympanic membrane and middle ear for differentiating otitis media," *Laryngoscope*, vol. 125, pp. E276–E282, 2015.

[22] H. R. Djalilian, J. Ridgway, M. Tam, A. Sepehr, Z. Chen, and B. J. Wong, "Imaging the human tympanic membrane using optical coherence tomography in vivo," *Otology Neurotology: Official Publication Amer. Otological Soc., Amer. Neurotology Soc. Eur. Acad. Otology Neurotology*, vol. 29, 2008, Art. no. 1091.

[23] J. Lee *et al.*, "Decalcification using ethylenediaminetetraacetic acid for clear microstructure imaging of cochlea through optical coherence tomography," *J. Biomed. Opt.*, vol. 21, 2016, Art. no. 081204.

[24] G. L. Monroy *et al.*, "Direct analysis of pathogenic structures affixed to the tympanic membrane during chronic otitis media," *Otolaryngology–Head Neck Surgery*, vol. 159, pp. 117–126, 2018.

[25] P. Pande, R. L. Shelton, G. L. Monroy, R. M. Nolan, and S. A. Boppart, "A mosaicking approach for in vivo thickness mapping of the human tympanic membrane using low coherence interferometry," *J. Assoc. Res. Otolaryngology*, vol. 17, pp. 403–416, 2016.

[26] K. Park *et al.*, "Optical assessment of the in vivo tympanic membrane status using a handheld optical coherence tomography-based otoscope," *Acta Oto-Laryngologica*, vol. 138, pp. 367–374, 2018.

[27] S. Han *et al.*, "Numerical-sampling-functionalized real-time index regulation for direct k-domain calibration in spectral domain optical coherence tomography," *Electronics*, vol. 7, 2018, Art. no. 182.

[28] R. E. Wijesinghe *et al.*, "Optically deviated focusing method based high-speed SD-OCT for in vivo retinal clinical applications," *Opt. Rev.*, vol. 23, pp. 307–315, 2016.

[29] K. Park *et al.*, "In vivo 3D imaging of the human tympanic membrane using a wide-field diagonal-scanning optical coherence tomography probe," *Appl. Opt.*, vol. 56, pp. D115–D119, 2017.

[30] C. T. Nguyen, H. Tu, E. J. Chaney, C. N. Stewart, and S. A. Boppart, "Non-invasive optical interferometry for the assessment of biofilm growth in the middle ear," *Biomed. Opt. Express*, vol. 1, pp. 1104–1116, 2010.

[31] C. T. Nguyen *et al.*, "Noninvasive in vivo optical detection of biofilm in the human middle ear," in *Proc. Nat. Acad. Sci.*, vol. 109, pp. 9529–9534, 2012.

[32] K. N. Chan, A. Silverstein, L. N. Bryan, C. E. McCracken, W. K. Little, and A. L. Shane, "Comparison of a smartphone otoscope and conventional otoscope in the diagnosis and management of acute otitis media," *Clin. Pediatrics*, vol. 58, pp. 302–306, 2019.

[33] G. L. Monroy *et al.*, "Non-invasive optical assessment of viscosity of middle ear effusions in otitis media," *J. Biophotonics*, vol. 10, pp. 394–403, 2017.

[34] R. Dsouza *et al.*, "In vivo detection of nanometer-scale structural changes of the human tympanic membrane in otitis media," *Scientific Rep.*, vol. 8, 2018, Art. no. 8777.

[35] W. Kim, S. Kim, J. S. Oghalai, and B. E. Applegate, "Endoscopic optical coherence tomography enables morphological and subnanometer vibratory imaging of the porcine cochlea through the round window," *Opt. Lett.*, vol. 43, pp. 1966–1969, 2018.

[36] L. Cai, G. Stomackin, N. M. Perez, X. Lin, T. T. Jung, and W. Dong, "Recovery from tympanic membrane perforation: Effects on membrane thickness, auditory thresholds, and middle ear transmission," *Hearing Res.*, vol. 384, 2019, Art. no. 107813.

[37] A. Starovoyt, T. Putzeys, J. Wouters, and N. Verhaert, "High-resolution imaging of the Human cochlea through the Round Window by means of optical coherence tomography," *Scientific Rep.*, vol. 9, pp. 1–10, 2019.

[38] J. Lee *et al.*, "Clinical utility of intraoperative tympanomastoidectomy assessment using a surgical microscope integrated with an optical coherence tomography," *Scientific Rep.*, vol. 8, pp. 1–8, 2018.

[39] N. Principi, P. Marchisio, C. Rosazza, C. Sciarrabba, and S. Esposito, "Acute otitis media with spontaneous tympanic membrane perforation," *Eur. J. Clin. Microbiology & Infectious Diseases*, vol. 36, pp. 11–18, 2017.

[40] O. B. Piltcher, J. D. Swarts, K. Magnuson, C. M. Alper, W. J. Doyle, and P. A. Hebda, "A rat model of otitis media with effusion caused by eustachian tube obstruction with and without Streptococcus pneumoniae infection: Methods and disease course," *Otolaryngology-Head Neck Surgery*, vol. 126, pp. 490–498, 2002.

[41] R. Dsouza *et al.*, "In vivo detection of nanometer-scale structural changes of the human tympanic membrane in otitis media," *Scientific Rep.*, vol. 8, pp. 1–13, 2018.

[42] M. Langston, A. Grobman, S. Goncalves, and S. I. Angeli, "Animal model of chronic tympanic membrane perforation," *Anatomical Rec.*, vol. 303, pp. 619–625, 2020.